Ultra-long spin relaxation in two-dimensional ferromagnet Cr 2 Ge 2 Te 6 flake

Article *in* 2D Materials · September 2021

DOI: 10.1088/2053-1583/ac2ab3

11 authors, including:

Chun Zhou
Arizona State University
15 PUBLICATIONS **59** CITATIONS
SEE PROFILE

Zhongzhu Jiang
University of Science and Technology of China
15 PUBLICATIONS **81** CITATIONS
SEE PROFILE

Zongwei Ma
Huazhong University of Science and Technology
43 PUBLICATIONS **834** CITATIONS
SEE PROFILE

Xuan Luo
Institute of Solid State Physics Chinese Academy of Sciences
179 PUBLICATIONS **3,626** CITATIONS
SEE PROFILE

2D Materials

PAPER

Ultra-long spin relaxation in two-dimensional ferromagnet $Cr_2Ge_2Te_6$ flake

RECEIVED
16 August 2021

REVISED
24 September 2021

ACCEPTED FOR PUBLICATION
27 September 2021

PUBLISHED
13 October 2021

Tao Sun[1,3,6], Chun Zhou[1,6], Zhongzhu Jiang[2,3], Xiaoming Li[1], Kang Qiu[4], Ruichun Xiao[4,*], Caixing Liu[1,3], Zongwei Ma[1], Xuan Luo[2], Yuping Sun[1,2,5] and Zhigao Sheng[1,*]

[1] Anhui Key Laboratory of Condensed Matter Physics at Extreme Conditions, High Magnetic Field Laboratory, HFIPS, Anhui, Chinese Academy of Sciences, Hefei 230031, People's Republic of China
[2] Key Laboratory of Materials Physics, Institute of Solid State Physics, HFIPS, Chinese Academy of Sciences, Hefei 230031, People's Republic of China
[3] University of Science and Technology of China, Hefei 230026, People's Republic of China
[4] Institutes of Physical Science and Information Technology, Anhui University, Hefei 230601, People's Republic of China
[5] Collaborative Innovation Center of Advanced Microstructures, Nanjing University, Nanjing, People's Republic of China
[6] These authors contributed equally to this work.
[*] Authors to whom any correspondence should be addressed.

E-mail: xiaoruichun@ahu.edu.cn **and** zhigaosheng@hmfl.ac.cn

Keywords: ultrafast spin dynamics, 2D van der Waals magnets, demagnetization, remagnetization, dimensionality, thermal diffusion anisotropy

Supplementary material for this article is available online

Abstract

By utilizing time-resolved magneto-optical Kerr effect technique, we investigated both demagnetization and remagnetization processes of a typical two-dimensional (2D) van der Waals (vdW) ferromagnetic (FM) semiconductor $Cr_2Ge_2Te_6$ (CGT) and two comparative Te-based crystals, i.e. three-dimensional (3D) FM metal Cr_3Te_4 (CT) and 2D vdW FM metal Fe_3GeTe_2 (FGT). Different from 3D CT showing one-step laser-induced demagnetization, two-steps demagnetization behavior is dominated in 2D vdW FGT and CGT, which indicates that the 2D vdW magnets have relatively weaker electron-spin coupling. Of particular interest, we discovered an ultra-long remagnetization behavior in the 2D vdW CGT flake. The laser pumping induced spin demagnetization would not recover even in the time scale of 3500 ps (experimental setup limitation). To the best of our knowledge, this is the longest remagnetization process observed so far and it might be one of the particular characterizations of *2D vdW ferromagnet semiconductors*. Based on the modified three temperature model, the key roles played by the crystal dimensionality and thermal diffusion anisotropy were revealed in the spin dynamics of 2D vdW magnets. Our findings would not only open the door to the thoroughly understanding of the origin of the magnetism in 2D FM materials but also undoubtedly find suitable applications in spintronics and magnonics devices.

1. Introduction

The two-dimensional (2D) van der Waals (vdW) magnet materials have layers structure with strong intralayer covalent bonding and weak vdW interlayer interactions [1, 2], and lead to the intralayer magnetic order may be retained to monolayer. Recently, 2D vdW materials, such as CrI_3, $Cr_2Ge_2Te_6$ (CGT), Fe_3GeTe_2 (FGT), have been experimentally shown to host long-range magnetic order until to atomic thickness [3–5], which provide unique opportunities for both fundamental physics and technological advances. Compared to three-dimensional (3D) cases, due to the weak vdW force and negligible substrate bonding, the spin of 2D vdW magnets can be easily modulated by various external stimulus, such as electric fields [6, 7], free carrier doping [8], strain [9, 10], and strong magnetic proximity effects [11]. This feature is very conducive to the development of miniaturized spintronics devices [12–14]. Accordingly, 2D magnets provide new platforms to probe the spin interaction with other degrees of freedom of electrons, as well as for novel spintronics applications. For instance, recent progresses in controllable

magnetism, giant magnetoresistance, and energy efficient switching, make 2D vdW magnetic tunnel junctions desirable for memory applications [15].

Promoted by ever-increasing operation speed of modern electronics, ultrafast spin dynamics has received great attentions in order to control magnetization from GHz to THz scale [16]. That also stimulates fundamental interests in the physics of magnetism in the ultrafast regime [17, 18]. It has been well established that the magnetization dynamics is a macroscopic manifestation of the quantum phenomenon of exchange coupling dynamics among spins [19], which is tightly associated with the anisotropy of the crystalline symmetry [20]. Compared with the 3D system, the 2D vdW magnetic material naturally has strong uniaxial magnetic anisotropy. Therefore, it is reasonable to deduce that the reduction of the exchange dimension between spins of 2D vdW magnets could lead to the emergence of unique spin dynamics behaviors compared to traditional 3D materials. By far, most of studies on 2D magnetic materials are focused on static and low-frequency behaviors [21–23], yet a few examples have been reported on the spin ultrafast dynamics of the 2D magnetic systems [24, 25], though the understanding spin dynamic is an essential task for the application of low dimensional spintronics devices.

Exploring the special characteristics of 2D vdW magnets' spin dynamics was the aim of the present work. Recently, laser-induced spin wave and its interfacial/electrostatic effects, has been investigated in 2D vdW magnet CrI_3 by Zhang *et al* [24]. In addition, Zhang *et al* reported the field dependence of the effective damping coefficient of spin waves in CGT [25]. Although the above reports have studied the spin characteristics of a special 2D vdW magnet in detail, they failed to explore how the decline in the dimension of the lattice structure would affect the spin dynamics from a global perspective. Here, by utilizing time-resolved magneto-optical Kerr effect (TR-MOKE) technique, we focused on the demagnetization and remagnetization processes of the 2D vdW magnets. In addition to the spin dynamic studying in the 2D vdW ferromagnetic (FM) semiconductor CGT, comparative experiments have also been done in 3D FM metal Cr_3Te_4 (CT) and 2D vdW FM metal FGT. Comparing with the 3D CT case, the two-steps demagnetization behavior of FGT and CGT indicates that the 2D vdW magnets have relatively weaker electron-spin coupling. On the other hand, the 2D vdW FGT and CGT have much longer remagnetization time than that of 3D CT crystal. An ultra-long spin relaxation was found in the 2D vdW FM semiconductor CGT and there is no obvious recovery of magnetism up to 3500 ps after laser-induced magnetization 100% quenching. To our best knowledge, this is the longest remagnetization process observed so far. These comparative results confirmed explicitly that the crystal dimensionality plays an important role in the spin dynamics of 2D vdW magnets.

2. Method

For the study of the ultrafast spin dynamics, a typical two-color TR-MOKE technique was utilized. The samples were placed in the cryostat (Oxford, 7 T SpectromagPT), which can provide a temperature environment of 1.5–300 K and a magnetic field environment of 0–7 T. The pump and probe laser beams were generated from a Ti:sapphire ultrafast laser (λ −800 nm, f −1 kHz). After laser pulses were divided into the pump and probe beams by a 3:7 plate beam splitter, converting the probe pulse wavelength to 400 nm with a nonlinear beta-barium borate crystal. The incident angle of the pump laser beam was ∼10°, while the probe beam monitored the response of the sample at a smaller angle from the normal to the sample (∼5°). The beams were focused onto the sample surface to a spot diameter of 400 and 300 μm by focusing lenses, for pump and probe, respectively, which were determined using a beam quality analyzer (Newport, LBP2-HR-VIS2). The energy density of a single probe pulse was chosen to be constant at 0.1 mJ cm^{-2} and the pump light was adjusted within the range of 0.79–1.99 mJ cm^{-2}. The time delay Δt between the pump and the probe pulses was controlled by adjusting a motorized translation stage on the pump optical path. During the TR-MOKE experiments, an external magnetic field was applied perpendicular to the sample plane, initiating the magnetization normal to the sample surface before each pump pulse reaches the sample. In this geometry, the MOKE signal measured with a balanced photodiode detector and lock-in amplified at 605 Hz, is proportional to the perpendicular magnetization component of the sample. To eliminate the influence of non-magnetic dynamics, only the part of the signal that changes sign upon magnetization reversal was taken into account by calculating the difference between the two MOKE signal transients corresponding to opposite field directions, i.e. Signal (+) − Signal (−).

3. Results and discussion

The 3D CT, 2D FGT and CGT flakes were grown by the flux methods [26]. In our experiments, the CGT and FGT thin flakes with a thickness of approximately 100 microns were used. In order to exclude the oxides' effect, the mechanical exfoliation method was utilized to create new oxide-free sample surfaces before our optical experiments. After the mechanical exfoliation, the CGT and FGT thin flakes with clean surfaces were immediately transferred into a sample chamber protected by helium gas.

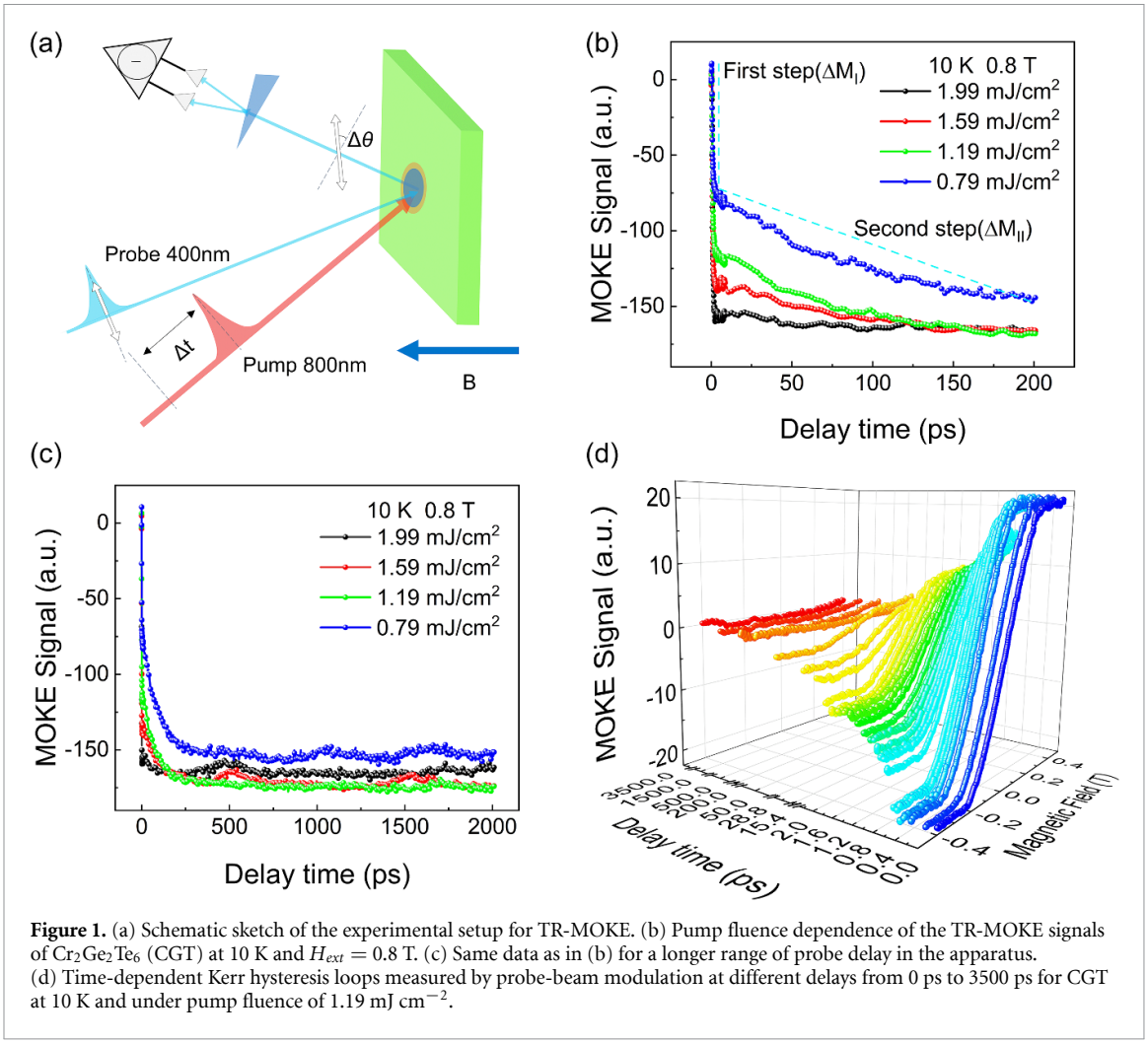

Figure 1. (a) Schematic sketch of the experimental setup for TR-MOKE. (b) Pump fluence dependence of the TR-MOKE signals of $Cr_2Ge_2Te_6$ (CGT) at 10 K and $H_{ext} = 0.8$ T. (c) Same data as in (b) for a longer range of probe delay in the apparatus. (d) Time-dependent Kerr hysteresis loops measured by probe-beam modulation at different delays from 0 ps to 3500 ps for CGT at 10 K and under pump fluence of 1.19 mJ cm^{-2}.

Their single-crystalline qualities and static magnetization properties were characterized and shown in supplementary information figures S1 and S2 (available online at stacks.iop.org/2DM/8/045040/mmedia). For the study of the ultrafast spin dynamics, the TR-MOKE technique was utilized as shown in figure 1(a). In this work, the CGT was chosen as a typical material for the studying of the ultrafast spin dynamics of the 2D vdW magnet. CGT is a FM semiconductor with space group *R*, and its Curie temperature is around 66 K [27, 28]. When a magnetic material is excited by a femtosecond laser pulse, the spin order can be completely or partially destroyed (demagnetization process) within a few hundred femtoseconds, and it is followed by a recovering process back to the original state (remagnetization) on a bit longer time scale. The TR-MOKE results of CGT are shown in figures 1(b) and (c), where the fluence of the pump pulse varies from 0.79 to 1.99 mJ cm^{-2} in steps of 0.4 mJ cm^{-2} at 10 K and $H_{ext} = 0.8$ T. After pumping by an ultrafast laser, the TR-MOKE signal experienced two steps of decline: an initial instantaneous decrease within several picoseconds (ps) and a subsequent slow decreasing response lasting for several hundreds of ps, indicating that the spin order continues to be destroyed after experienced first step of decline. Decades before, it has been found that the demagnetization in Gd proceeds within 100 ps (two-steps) [29], while it becomes three orders of magnitude faster in FM 3d transition metals (one-step) such as Ni [30]. In order to discuss this issue conveniently, Koopmans *et al* classified the demagnetization process as two types. Type-I depicts the single-step demagnetization in the magnetic materials with a large spin-flip rate and type-II characters the two-step demagnetization in the magnetic material with a small spin-flip rate [31]. Accordingly, the demagnetization process observed here in 2D vdW magnet CGT is a typical type-II dynamics [31]. This indicates that the demagnetization efficiency is insufficient to establish a full thermal equilibrium of the spin system during electron-phonon equilibration [32]. With the increase of the pump fluences, the second step of the demagnetization process gradually disappears. This means that the demagnetization process gradually transitions from type-II dynamics to type-I dynamics.

In previous laser-induced femtosecond experiments, much effort has been devoted to the demagnetization process, and less attention has been paid

to the aspect of the recovery of magnetism after a material has been subjected to a strong femtosecond pulse despite its equal importance for future working devices [33]. Here, after checking the demagnetization process, we paid special attention to the remagnetization behavior of the 2D vdW magnet. The TR-MOKE signals on a much longer time scale are shown in figure 1(c). It is surprising to find that the MOKE signals do not show any recovering tendencies within 2000 ps and even 3500 ps (experimental setup limitation, as seen in supplementary information figure S3). Moreover, such ultra-long remagnetization behavior happens in the whole temperature regime below T_C (supplementary information figure S6).

In general, the laser pumped spin system in the 3D FM metals would recover within several hundred picoseconds [33, 34]. Recently, it has been reported that there exists relative longer spin remagnetization behavior in magnetic metal heterojunctions and diluted magnetic semiconductors. For instance, the remagnetization of Fe/Gd multilayer film is long, and it can only recover approximately 60% at 2000 ps after pumping by Eimüller *et al* [35]. Moreover, Héroux *et al* found that the diluted magnetic semiconductor GaMnAs possesses longer spin relaxation time compared to the other materials and there is only about 20% of the magnetic recovery can be achieved at 2000 ps after being excited by a pulsed laser [36]. In our experiment, the magnetization of the 2D vdW magnet CGT does not show any recovering within the limits of the time scale we can observe (∼3500 ps). To the best our knowledge, it is the longest remagnetization process observed so far [30, 37, 38], which might be one of the particular characterizations of 2D vdW FM semiconductors.

To further explore both the demagnetization and remagnetization processes of 2D magnet CGT, the MOKE hysteresis loops were measured by varying delay times (0–3500 ps) between the pump and probe laser beams. The typical results obtained at 10 K with a pump fluence of 1.19 mJ cm^{-2} are shown in figure 1(d). It is found that the full magnetization (100%) of CGT drops fast down to 43.5% within 1.8 ps, which corresponds to the step I demagnetization. It is followed by a slower demagnetization (step II) and the magnetization of CGT decreases slowly down to 0% (fully demagnetized) when delay time reaches 200 ps. Such a fully quenched state keeps until our delay stage goes to the end (∼3500 ps). These results demonstrate that (a) as the hysteresis loop curve becomes flat, its magnetization is nearly 100% quenched by ultrafast laser pumping, (b) CGT indeed has an ultra-long relaxation time after laser excitation, being consistent with the previous results (figure 1(c)). It is worth mentioning that 3500 ps is our measurement limitation, so the relaxation time should be longer than it.

Magnetization dynamics is a macroscopic manifestation of the quantum phenomenon of exchange coupling dynamics between spins [19]. The spin dynamics is tightly related to both magnetic anisotropy and the thermal energy dissipation of the material [20, 29, 39, 40]. Different from the 3D system, the 2D vdW magnets naturally have strong anisotropy for both magnetic interaction and the thermal energy dissipation rate due to the existence of vdW gap [3, 41]. In order to further explore the spin dynamics of the 2D vdW magnet, two additional Te-based magnetic materials (CT and FGT) were chosen to study for comparison. As shown in figure 2(a), CT is a FM metal with a 3D crystal structure and FGT is a FM metal with a 2D vdW crystal structure. The same kind of TR-MOKE experiments were done for both CT and FGT flakes and the typical demagnetization and remagnetization data obtained with a pump fluence of 1.19 mJ cm^{-2} were collected in figures 2(b) and (d), respectively. More details can be found in supplementary information figure S4. It was found that the spin demagnetizations after laser pumping of CT and FGT are much fast than that of CGT (figure 2(b)). The TR-MOKE signal of CT drops down to a minimum within 1.3 ps and then recovers soon. This one-step behavior indicates it is a typical type-I dynamic process [31] and 3D FM CT has relative stronger electron-spin coupling. As for the 2D FM FGT, a fast demagnetization in the first picoseconds is followed by a slower demagnetization, which suggests that the temperature of the electron system in this 2D spin system is different for the first picoseconds compared to the latter. Though the two-step characterization (type-II demagnetization) features are similar to each other, the total demagnetization process of FGT (∼70 ps) is much faster than that of CGT (∼200 ps).

We measured the TR-MOKE signals of three samples at different pump fluences, finding that the pump fluence can change the TR-MOKE signal curves (see details in supplementary information figure S4). In order to quantitatively describe the differences of the demagnetization process among the three samples, a physical quantity w_{II}, which characterizes the contribution of the second step demagnetization to the whole demagnetization process, is introduced as

$$w_{II} = \frac{\Delta M_{II}}{\Delta M_I + \Delta M_{II}}, \quad (1)$$

where ΔM_I denotes the first step demagnetization amplitude of MOKE signal, and ΔM_{II} denotes the second step demagnetization amplitude of MOKE signal. As shown in figure 2(c), the w_{II} of CT is always towards to zero with different pump fluence, which indicates that the demagnetization process of CT is a robust type-I dynamics process. For 2D FGT and CGT, which initially possess the type-II demagnetization behaviors, the increasing of pump fluence can reduce the w_{II} value dramatically. For instance, when pump fluence is larger than 1.59 mJ cm^{-2}, the w_{II} of FGT nearly decline to 0. This indicates that a high

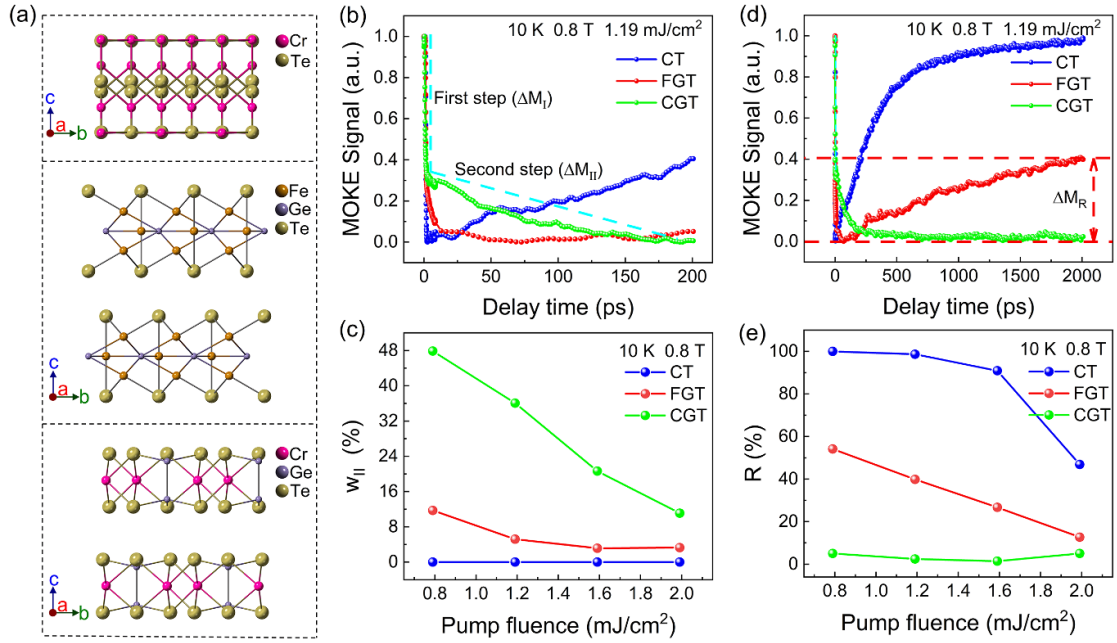

Figure 2. (a) Crystal structure of Cr_3Te_4 (CT), Fe_3GeTe_2 (FGT), and $Cr_2Ge_2Te_6$ (CGT). (b) TR-MOKE signals of three samples at 10 K, under a pump fluence of 1.19 mJ cm^{-2} and a 0.8 T out-of-plane field. (c) The ratio of the demagnetization amplitude of the second step to the total demagnetization amplitude (w_{II}) as a function of pump fluence. (d) Same data as in (b) for a longer range of probe delay. (e) The recovery ratio of magnetization (R) at 2000 ps time delay as a function of the pump fluence at 10 K, and an out-of-plane applied field of 0.8 T.

energy pump laser can drives the spin demagnetization of 2D vdW magnet from type-II to type-I, which is consistent with the behaviors of some FM materials such as GaMnAs, InMnAs [37, 42] and contrary to the behaviors of Co and Ni [31].

The ultrafast demagnetization is microscopically caused by the spin flip of electron at the Fermi level ε_F, which is mediated by an Elliott–Yafet (E–Y) type of electron-phonon scattering process [31], and the process is accompanied by the transfer of energy from the electron to the spin system [32]. The demagnetization usually shows a type-I dynamics process when the electron and spin system are strongly coupled. On the contrary, the weak electron-spin coupling will lead to type-II dynamics process [32], and more details can be found in supplementary information figure S5. For 3D metallic FM, the electron is itinerant and the motion of the electron in the 3D direction is not restricted, which means that it has a very high electron-phonon scattering rate and the coupling of the spin to electron system is strong. As a result, the demagnetization processes of 3D metal FM CT and the previously reported Co [43], Ni [30, 44], Fe [45], FePt [40] all belong to type-I dynamics. For the 2D semiconductor FM such as CGT, the semiconductor properties make the Fermi level lack electrons, which leads to the weaker electron-spin coupling compared with the 3D metallic FM. Therefore, the demagnetization process of 2D semiconductor FM CGT shows the characteristics of type-II dynamics. For FGT, its electrons are non-local and it also has the similar conductivity to CT (the resistivity of CT is only 140 $\mu\Omega$·cm at the 4 K temperature [46], for FGT, 136.5 $\mu\Omega$·cm at the 10 K temperature [47]), however, due to the existence of vdW gaps, the E–Y scattering of electrons between layers is bound to be limited. Consequently, the overall electron-spin coupling strength is weaker than that of 3D metals, and its ultrafast demagnetization behavior resides in the transition region between type-I and type-II dynamics behavior. As a semiconductor, the conductivity of CGT increases with temperature and its demagnetization behavior at high temperatures should be similar to that of FGT. In order to confirm this scenario, additional temperature dependent TR-MOKE experiments were done for 2D vdW CGT flakes. It was found that as the temperature increases, the w_{II} of CGT is monotonously smaller as expected (supplementary information figure S6).

Figure 2(d) shows the spin dynamics of three samples within 2000 ps. It is evident that the remagnetization processes of the three samples also have obvious differences. 3D FM CT has the fastest rate of remagnetization among the three samples, and the recovery of magnetization can achieve up to 80% at 500 ps and 98% at 2000 ps. Compared with CT, the remagnetization rate of FGT is relative slower, and the recovery ratio is only 40% at 2000 ps. The remagnetization time of CGT is the longest, and no significant magnetic recovery was

observed within 2000 ps. Similar to the description of demagnetizations, a magnetization recovery ratio R is introduced as

$$R = \frac{\Delta M_{\mathrm{R}}}{\Delta M_{\mathrm{D}}}, \quad (2)$$

where ΔM_{D} denotes the maximum demagnetization amplitude of the MOKE signal and ΔM_{R} means the MOKE signal at 2000 ps. Figure 2(e) exhibits the pump laser fluence dependence of R for three samples obtained at 10 K and 0.8 T. With increasing of pump fluence, higher electron and lattice temperatures can be achieved, thus leading to a relatively longer spin-lattice relaxation time and recovery process. As shown in figure 2(e), it is reasonable to find that the R value of both 3D CT and 2D FGT decreases with increasing of pump fluences. For the 2D FM semiconductor CGT, the R value does not show a significant correlation with pump fluence, and its value remain near 0.

According to the TR-MOKE studies of CT, FGT, and CGT above, it can be found that the spin dynamics, especially remagnetization process, are tightly related to both the crystal dimensionality and thermal dissipation ability of the materials. In order to explain the spin dynamic behaviors of FM metals, Beaurepaire *et al* introduced a phenomenological 3TM, describing the interaction between the electron, spin and lattice sub-systems [30]. Later, Hübner proposed an additional channel for ultrafast transfer between spin and orbital momenta [29] and Koopmans *et al* addressed the dissipation of angular momentum [48], which is both greatly improved the applicability of the 3TM model. According to this model, the spin remagnetization correspond to a thermal energy diffusion process from the laser heated hot spot.

In previous studies, the crystal dimensionality related thermal energy dissipation anisotropy was not considered. As for our case, obviously, it cannot be ignored. In order to qualitative understand the crystal dimensionality effect on remagnetization behavior, the thermal diffusion process of three typical models with different thermal conductivity parameters were considered. As illustrated in figures 3(a)–(c), the red region is at a high temperature and the spins are disordered, and the blue region is at a low temperature and the spins are ordered. For the 3D model with isotropic and high thermal conductivity (high κ) represented by CT, thermal energy can rapidly diffuse away from the hot spot at an isotropic and fast speed, which causes the temperature to decrease and spin order recover at hot spot. After experiencing 2000 ps of thermal diffusion, the magnetization and temperature at the hot spot has basically recovered to the state before excitation (figure 3(a)). For the 2D model with anisotropy and high thermal conductivity (high κ) (figure 3(b)), such as situation happening in 2D metallic FGT, thermal energy can diffuse away from the hot spot at an anisotropic speed (it has high in-plane thermal conductivity and low interlayer thermal conductivity). Therefore, it has a slower spin relaxation rate than the first model. For the 2D semiconductor CGT case, the laser-induced spin dynamic should be consistent with the 2D model with anisotropy and low thermal conductivity (low κ). The thermal energy generated by laser irradiation is limited to hot spots and it is difficult to diffuse outward. At the same time, the two subsystems of spin and lattice are tightly combined by strong spin-phonon coupling interaction which was first confirmed by Tian *et al* through high-resolution micro-Raman scattering measurements [49]. Based on the above reasons, the spin at the hot spot is disorder for a long time (figure 3(c)).

We used the heat conduction theory to simulate the heat conduction process of above three typical models and more details can be found in supplementary information S10. The simulation results are shown in figure 3(d). It can be found that the thermal conductivity can effectively affect the thermal dynamics at the hot spot. For 3D model with isotropy and high thermal conductivity, the temperature at the hot spot drops swiftly, while for the model with quasi-2D anisotropy and low thermal conductivity, the temperature at the hot spot is basically invariant. Therefore, the ultra-long spin relaxation of CGT may be caused by the ultra-long thermal diffusion process of the hot spot.

Although the strong anisotropy of thermal diffusion caused by 2D characteristics can qualitatively and reasonably explain the long relaxation time, its microscopic mechanism still needs to be further explored. Charge and spin are two degrees of freedom of the electron. Not only the static one, but also the dynamic behaviors of spin and charge may couple to each other. In general, the dynamic behavior of electron charge is directly related to the reflectivity of the materials [50]. In order to explore the unusual spin dynamic behaviors of the 2D vdW materials further, the TR reflectance of CT, FGT, and CGT were studied. The typical results obtained at 10 K with magnetic field ~0.8 T and pump fluence ~1.19 mJ cm^{-2} are shown in figure 3(e). It can be found that, after laser pumping, the reflectance of 3D magnet CT gets a sudden change and recover back to its initial state within 500 ps, which is quite similar to its spin dynamic behavior (figure 2(d)). As for the 3D FM metal FGT, the recovery of reflectance needs more long time (~2000 ps). Contrarily, the laser pumping induced sudden reflectance change of 2D FM semiconductor CGT is partially recovered within the first 10 ps, and then it is no obvious recovery process in the next 2000 ps time delay, which indicates that the temperature at the hot spot has been maintained at a high temperature.

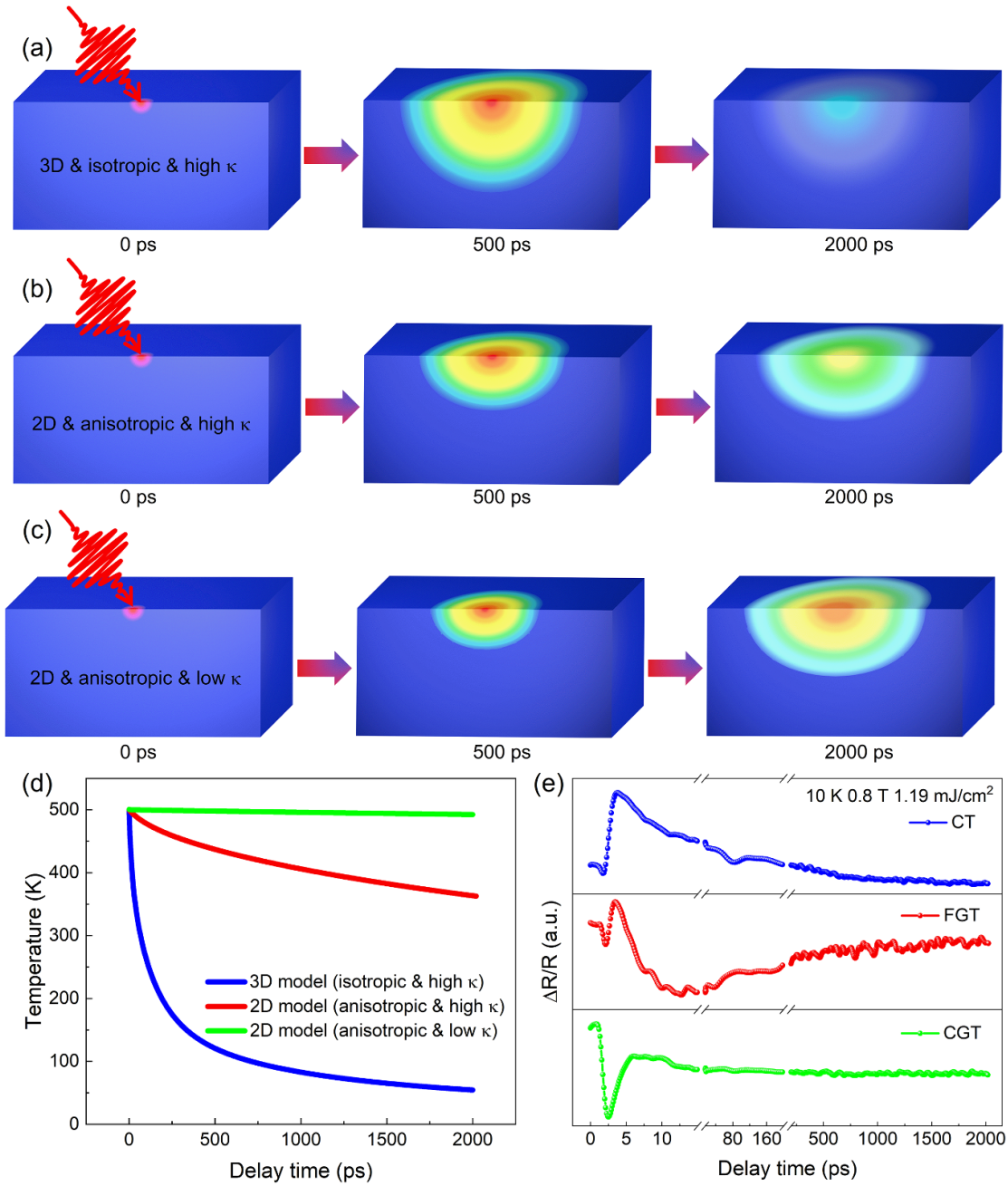

Figure 3. (a)–(c) Schematic diagram of spin relaxation of three models (3D model with isotropic and high thermal conductivity (high κ), quasi-2D model with anisotropic and high thermal conductivity (high κ), and quasi-2D model with anisotropic and low thermal conductivity (low κ)) at different time points after being excited by laser, the red region's spins are disordered, the blue region's spins are ordered. (d) The thermal diffusions of three typical models with different thermal conductivity parameters were simulated by heat conduction theory, where the initial temperature at the hot spot was 500 K and the ambient temperature was 10 K. (e) The transient reflectivity $\Delta R/R$ curves of three samples at 10 K, under a pump fluence of 1.19 mJ cm^{-2} and a 0.8 T out-of-plane field.

4. Conclusion

Ultrafast laser induced both demagnetization and remagnetization of 3D FM metal CT, 2D FM metal FGT, and 2D FM semiconductor CGT have been investigated by means of TR-MOKE technique. Contrasting to the one-step demagnetization in 3D CT, both 2D magnets FGT and CGT show two-steps demagnetization behavior, which indicates that the 2D vdW magnets have relative weaker electron-spin coupling. Moreover, the remagnetization of 2D vdW magnets is much slower than that for 3D magnet CT. It is intriguing to find that there is no obvious recovery of CGT's magnetism in the time scale of 3500 ps (limited by experimental setup) after ultrafast demagnetization. These features obtained by such comparative experiments reveal that the crystal dimensionality and thermal diffusion anisotropy play key roles in the spin dynamics. These results were partially understood and simulated by a modified 3TM. Our finding would not only be benefic for the better understanding of the 2D magnetization but also undoubtedly

find suitable applications in spintronic and magnonic devices.

Data availability statement

All data that support the findings of this study are included within the article (and any supplementary files).

Acknowledgments

We gratefully acknowledge financial support from the National Key R&D Program of China (Grant Nos. 2017YFA0303603 and 2016YFA0401803), the National Natural Science Foundation of China (NSFC; Grant Nos. U2032218, 11574316, 11947212, 61805256, and 11904367), the Plan for Major Provincial Science & Technology Project (Grant No. 202003a05020018), the Key Research Program of Frontier Sciences, CAS (Grant No. QYZDB-SSW-SLH011), and Users with Excellence Program of Hefei Science Center CAS (Grant No. 2021HSC-UE009). A portion of this work was performed on the Steady High Magnetic Field Facilities (Ultrafast optical measurement system under superconducting magnet), High Magnetic Field Laboratory, CAS and supported by the High Magnetic Field Laboratory of Anhui Province.

Conflict of interest

The authors declare no competing financial interest.

ORCID iDs

Tao Sun https://orcid.org/0000-0002-4355-2425
Zhongzhu Jiang https://orcid.org/0000-0002-8317-0181
Ruichun Xiao https://orcid.org/0000-0001-8085-2251
Zongwei Ma https://orcid.org/0000-0002-9328-9194
Xuan Luo https://orcid.org/0000-0002-0482-4096
Zhigao Sheng https://orcid.org/0000-0003-3382-5968

References

[1] Withers F *et al* 2015 *Nat. Mater.* **14** 301–6
[2] Lin Z *et al* 2016 *2D Mater.* **3** 21
[3] Gong C *et al* 2017 *Nature* **546** 265–9
[4] Huang B *et al* 2017 *Nature* **546** 270
[5] Fei Z *et al* 2018 *Nat. Mater.* **17** 778–82
[6] Jiang S, Shan J and Mak K F 2018 *Nat. Mater.* **17** 406
[7] Xing W Y *et al* 2017 *2D Mater.* **4** 7
[8] Seyler K L *et al* 2018 *Nano Lett.* **18** 3823–8
[9] Li T *et al* 2019 *Nat. Mater.* **18** 1303
[10] Song T *et al* 2019 *Nat. Mater.* **18** 1298
[11] Zhong D *et al* 2017 *Sci. Adv.* **3** 6
[12] Ohno H, Chiba D, Matsukura F, Omiya T, Abe E, Dietl T, Ohno Y and Ohtani K 2000 *Nature* **408** 944–6
[13] Wang Z, Tang C, Sachs R, Barlas Y and Shi J 2015 *Phys. Rev. Lett.* **114** 016603
[14] Xiao R-C, Shao D-F, Li Y-H and Jiang H 2021 *npj Quantum Mater.* **6** 35
[15] Yang W, Cao Y, Han J, Lin X, Wang X, Wei G, Lv C, Bournel A and Zhao W 2021 *Nanoscale* **13** 862–8
[16] Luo J, Zheng H, Shen C, Zhang H, Zhu K, Zhu H, Liu J, Li G, Ji Y and Zhao J 2010 *Sci. China Phys. Mech.* **53** 779–82
[17] Zhao B, Xue H, Wu G, Zhu Z, Ren Y, Jin Q Y and Zhang Z 2019 *Appl. Phys. Lett.* **115** 062401
[18] Xia H *et al* 2021 *Phys. Rev.* B **104** 024404
[19] Batignani G, Bossini D, di Palo N, Ferrante C, Pontecorvo E, Cerullo G, Kimel A and Scopigno T 2015 *Nat. Photon.* **9** 506–10
[20] Li Y *et al* 2021 *J. Phys.: Condens. Matter* **33** 7
[21] Huang M *et al* 2021 *2D Mater.* **8** 8
[22] Leon A M, Gonzalez J W, Mejía-López J, Crasto de Lima F and Suárez Morell E 2020 *2D Mater.* **7** 7
[23] Yi J Y *et al* 2017 *2D Mater.* **4** 6
[24] Zhang X-X, Li L, Weber D, Goldberger J, Mak K F and Shan J 2020 *Nat. Mater.* **19** 838–42
[25] Zhang T, Chen Y, Li Y, Guo Z, Wang Z, Han Z, He W and Zhang J 2020 *Appl. Phys. Lett.* **116** 223103
[26] Hao Z Q, Li H W, Zhang S, Li X, Lin G, Luo X, Sun Y, Liu Z and Wang Y 2018 *Sci. Bull.* **63** 825–30
[27] Selter S, Bastien G, Wolter A U B, Aswartham S and Büchner B 2020 *Phys. Rev.* B **101** 014440
[28] Zeisner J, Alfonsov A, Selter S, Aswartham S, Ghimire M P, Richter M, van den Brink J, Büchner B and Kataev V 2019 *Phys. Rev.* B **99** 165109
[29] Hubner W and Bennemann K H 1996 *Phys. Rev.* B **53** 3422–7
[30] Beaurepaire E, Merle J-C, Daunois A and Bigot J-Y 1996 *Phys. Rev. Lett.* **76** 4250–3
[31] Koopmans B, Malinowski G, Dalla Longa F, Steiauf D, Fähnle M, Roth T, Cinchetti M and Aeschlimann M 2010 *Nat. Mater.* **9** 259–65
[32] Roth T *et al* 2012 *Phys. Rev.* X **2** 021006
[33] Kazantseva N, Nowak U, Chantrell R W, Hohlfeld J and Rebei A 2008 *EPL (Europhys. Lett.)* **81** 27004
[34] Mendil J, Nieves P, Chubykalo-Fesenko O, Walowski J, Santos T, Pisana S and Münzenberg M 2014 *Sci. Rep.* **4** 3980
[35] Eimuller T, Scholl A, Ludescher B, Schütz G and Thiele J-U 2007 *Appl. Phys. Lett.* **91** 042508
[36] Heroux J B *et al* 2005 Ultrafast magneto-optical spectroscopy of GaMnAs *Bellingham SPIE-Int. Soc. Optical Engineering* (https://doi.org/10.1117/12.601978)
[37] Wang J, Sun C, Kono J, Oiwa A, Munekata H, Cywiński Ł and Sham L J 2005 *Phys. Rev. Lett.* **95** 167401
[38] Zhang W, Liu Q, Yuan Z, Xia K, He W, Zhan Q-F, Zhang X-Q and Cheng Z-H 2019 *Phys. Rev.* B **100** 104412
[39] Song H-S, Lee K-D, Sohn J-W, Yang S-H, Parkin S S P, You C-Y and Shin S-C 2013 *Appl. Phys. Lett.* **103** 022406
[40] Willig L, von Reppert A, Deb M, Ganss F, Hellwig O and Bargheer M 2019 *Phys. Rev.* B **100** 224408
[41] Kim K, He J, Ganeshan B and Liu J 2018 *J. Appl. Phys.* **124** 055104
[42] Zahn J P, Gamouras A, March S, Liu X, Furdyna J K and Hall K C 2010 *J. Appl. Phys.* **107** 033908
[43] Cinchetti M, Albaneda M S, Hoffmann D, Roth T, Wüstenberg J-P, Krauß M, Andreyev O, Schneider H C, Bauer M and Aeschlimann M 2006 *Phys. Rev. Lett.* **97** 4
[44] Dalla Longa F, Kohlhepp J T, de Jonge W J M and Koopmans B 2007 *Phys. Rev.* B **75** 224431
[45] Carpene E, Mancini E, Dallera C, Brenna M, Puppin E and de Silvestri S 2008 *Phys. Rev.* B **78** 174422
[46] Babot D and Chevreton M 1973 *J. Solid State Chem.* **8** 166–74
[47] Chen B, Yang J, Wang H, Imai M, Ohta H, Michioka C, Yoshimura K and Fang M 2013 *J. Phys. Soc. Japan* **82** 124711
[48] Koopmans B, Ruigrok J J, Longa F D and de Jonge W J M 2005 *Phys. Rev. Lett.* **95** 267207
[49] Tian Y, Gray M J, Ji H, Cava R J and Burch K S 2016 *2D Mater.* **3** 025035
[50] Caffrey A P, Hopkins P E, Klopf J M and Norris P M 2005 *Microscale Thermophys. Eng.* **9** 365–77